Energy Reports 7 (2021) 8849–8857

Contents lists available at ScienceDirect

Energy Reports

journal homepage: www.elsevier.com/locate/egyr

Research paper

# A load frequency control strategy based on disturbance reconstruction for multi-area interconnected power system with hybrid energy storage system

Feng Zhu [a], Xichao Zhou [b], Yiwei Zhang [c], Dezhi Xu [c,*], Jingqi Fu [a]

[a] School of Mechatronic Engineering and Automation, Shanghai University, Shanghai 200444, China
[b] Science and Technology Research and Development Center, State Grid Integrated Energy Service Group Co., Ltd. Beijin 100053, China
[c] School of Internet of Things Engineering, Jiangnan University, Wuxi 214122, China

ARTICLE INFO

*Article history:*
Received 8 April 2021
Received in revised form 27 August 2021
Accepted 11 September 2021
Available online 30 November 2021

*Keywords:*
Load frequency control (LFC)
Hybrid energy storage system (HESS)
Interval observer
Disturbance reconstruction

ABSTRACT

In order to handle the problem of frequency fluctuations caused by load disturbances in multi-area interconnected power systems, a sliding mode control strategy for hybrid energy storage system has been designed by combining interval observer and disturbance reconstruction technology. The hybrid energy storage system composed of a battery and a super capacitor has been used to improve the performance of load frequency control systems. Using the load frequency control model of the multi-area interconnected power system, the interval observers are designed for each area to get the information about interval bounds of the system state in each area online. Then, the load disturbance in each area is reconstructed online using the estimation information of system state, and a sliding mode controller based on interval disturbance reconstruction is designed for power consumption and storage of the hybrid energy storage system, so as to stabilize the power grid frequency. Simulation results have shown that the proposed control strategy can effectively suppress the frequency and tie-line power fluctuations caused by load disturbances, and ensure the reliability and stability of the power system.

© 2021 The Authors. Published by Elsevier Ltd. This is an open access article under the CC BY-NC-ND license (http://creativecommons.org/licenses/by-nc-nd/4.0/).

## 1. Introduction

At present, fossil energy depletion and environmental pollution are still a major challenge facing mankind. In order to gradually replace fossil energy power generation, the renewable energy like photovoltaic is developed and utilized in the field of power system due to significant advantages like renewability and environmental friendliness (Parvaneh and Khorasani, 2020). However, with the large-scale integration of renewable energy into the power system, its weak inertia, volatility and uncertainty, as well as some inherent disadvantages of traditional generator sets, make it more challenging to maintain the nominal frequency and stabilize the system performance (Alhelou and Golshan, 2019).

In contrast to a traditional centralized power supply system, the modern power grid consists of multiple interconnected subsystems. All grid areas are highly interconnected, and the power grid is protected, monitored and controlled through various communication equipments (Ameli and Hooshyar, 2018). Frequency stability is an important indicator of power quality in power systems. At present, the main method to improve the stability of power grid frequency is load frequency control. However, due to the uncertainty of active power production caused by the integration of large-scale renewable energy into the power grid, the power grid frequency is highly oscillated, so improving the robustness of LFC method has become a challenge (Alhelou and Golshan, 2018). In response to this challenge, various LFC methods have been proposed since the 1970s (Saikia et al., 2011; Rubaai and Udo, 1992; Rahmani and Sadati, 2013; Wang et al., 2018; Mi et al., 2016; Rerkpreedapong et al., 2003; Onyeka et al., 2020). In Wang et al. (2018) and Mi et al. (2016), a sliding mode control strategy based on disturbance observer is designed to improve the robustness of the system and reduce the frequency deviation. In Onyeka et al. (2020), a decentralized sliding mode controller has been designed for LFC system with time-delay problems, which improves the robustness of the system. This method has provided a reliable solution for systems with random disturbances and time-varying delays. In Alhelou and Golshan (2020), a fully decentralized LFC approach based on dynamic state estimation is proposed to track the running state of the system in real time and improve the robustness of the system. In addition, in the new environment of modern power system development, power grid frequency stability is facing many new challenges.

* Corresponding author.
*E-mail address:* xudezhi@jiangnan.edu.cn (D. Xu).

https://doi.org/10.1016/j.egyr.2021.09.029
2352-4847/© 2021 The Authors. Published by Elsevier Ltd. This is an open access article under the CC BY-NC-ND license (http://creativecommons.org/licenses/by-nc-nd/4.0/).

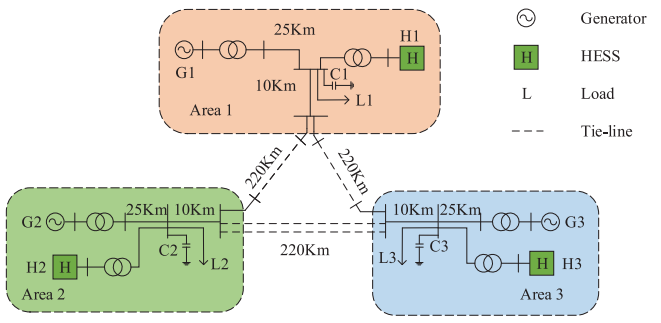


**Fig. 1.** Three-area power grid with HESS.

Therefore, introducing higher quality frequency modulation resources to solve the problem of power grid frequency stability has become a hot research topic.

With the development of energy storage technology, researchers have found that the introduction of energy storage systems into modern power grids can improve the frequency stability of the system (Xu et al., 2018; Yang et al., 2019; Zhou et al., 2020; Tungadio and Sun, 2019). In the power grid, the energy storage part is usually devoted to stabilize the power fluctuation, and enhances the power quality of the system (Gholami and Parvaneh, 2019). In many types of high-efficiency energy storage systems, the HESS composed of super-capacitors and batteries has the right combination of high power density, short charge and discharge time, high reliability, and long cycle life. It is more suitable for power systems with high power and frequent charging and discharging, and is widely regarded as an effective way to smooth the fluctuations of power in power system. In Xu et al. (2018), an identifier and controller have been designed by utilizing two kinds of neural networks to improve a four-area interconnected LFC system with the HESS and maintain system frequency stability. In Yang et al. (2019) and Zhou et al. (2020), for the HESS actuator fault problem in the interconnected power system, a fault-tolerant control strategy has been designed to ensure the safe operation of the system in the case of load disturbance and actuator fault. Yan et al. (2018) has proposed a $H_\infty$ robust controller for a HESS in order to improve the performance of frequency modulation. Based on the above research, we find that the application of HESS to LFC of interconnected power system is a topic worthy of research.

In the multi-area interconnected power system, external disturbance is inevitable. In the case of external disturbance or mismatch between the model and the actual system, interval observer has been proven to be an effective state estimation strategy since it has been applied to solve some practical problems and handle large uncertainties (Su et al., 2020; Tian et al., 2020; Zhang and Yang, 2017). In Su et al. (2020), the interval observer has been introduced to design a fault detection scheme for the switching system. Tian et al. (2020) has investigated the problem of fault estimation of high-speed railway traction motor based on interval observer. Zhang and Yang (2017) has used interval observer to study the fault detection of discrete linear variable parameter systems with bounded disturbances. The advantages of interval observers when applied to state estimation are examined in Li et al. (2019). Zammali et al. (2020) is concerned with sensor fault detection for switched systems by using interval observer with $L_\infty$ performance. However, the reconstruction of unknown inputs through interval observation technology is still an open problem.

Motivated by the aforementioned discussion, this paper has proposed an improved sliding mode load frequency control based on interval observer for LFC system with HESS. Interval observers has been designed for LFC system to realize the interval estimation of the state in each area. Then, using this kind of interval information to realize the estimations of system load disturbances. Moreover, the sliding mode controller, which takes the load disturbances into account, supplies the desired and appropriate power flow reference for HESS. Furthermore, the stability analysis of the whole closed-loop system is presented for the proposed controller by Lyapunov theory. The simulation results show that the disturbance reconstruction method proposed in this paper can quickly and accurately obtain the load disturbance reconstruction values in each area without the accurate disturbance boundary values. And, under the control strategy proposed here, the HESS effectively participates in frequency modulation to ensure the stability of the power grids, and maintain the system frequency and tie line power fluctuations within a small range.

The rest is arranged as follows. In Section 2, the LFC of a power grid with a HESS and some preliminary definitions and work are presented. The interval observer-based disturbance reconstruction technology and the sliding model controller based on for the HESS, are presented in Section 3. The Section 4 gives the simulation experiment and result analysis. Finally, we describe the conclusion in Section 5.

## 2. Problem formulation and preliminaries

In the traditional LFC system, automatic generation control (AGC) is used as its secondary controller. Adjustment of the grid frequency is done by adjusting the set value of the power plant governor (Wood and Wollenberg, 2012). To improve the unstable frequency quality, which is caused by the connection of a large number of new energy sources in recent years, this paper takes a three-area power grid as an example of an interconnected power system after the introduction of a HESS. A three-area power grid with a HESS is shown in Fig. 1. Each area is mainly composed of power generation system, user load, and HESS, and power exchanges between different areas through tie lines.

### 2.1. The HESS modeling

To eliminate the negative impact of the power system's fluctuating power, we here use a HESS composed of a battery and a super-capacitor, to adjust the grid's fluctuating power. The control structure of a HESS is shown in Fig. 2. In this paper, a low-pass filter is used for power distribution. Among the HESS components, the battery has high energy density and is responsible for the part of low-frequency load disturbances, and the super-capacitor charges and discharges quickly, and bears the high-frequency part.

$$P_B^*(t) = u^*(t) - RC\frac{dP_B^*(t)}{dt} \tag{1}$$

$$P_C^*(t) = u^*(t) - P_B^*(t) \tag{2}$$

where $u^*(t)$ is the output of the controller; $RC$ is the Low-pass filter parameters; $P_B^*(t)$ is the control command to the battery; $P_C^*(t)$ is the control command to the super-capacitor.

According to the charge and discharge characteristics of HESS, the models of super-capacitor and battery can express as follows:

$$\frac{di_C}{dt} = -\frac{R_C}{L_C}i_C + \frac{1}{L_C}u_C - \frac{m_{12}}{L_C}u_{DC}, m_{12} = \begin{cases} 1-m_1 & i_C > 0 \\ m_2 & i_C < 0 \end{cases} \tag{3}$$

$$\frac{di_B}{dt} = -\frac{R_B}{L_B}i_B + \frac{1}{L_B}u_B - \frac{m_{34}}{L_B}u_{DC}, m_{34} = \begin{cases} 1-m_3 & i_B > 0 \\ m_4 & i_B < 0 \end{cases} \tag{4}$$

where $m_i$ means the duty cycle of the IGBT $S_i$, which varies form 0 to 1.

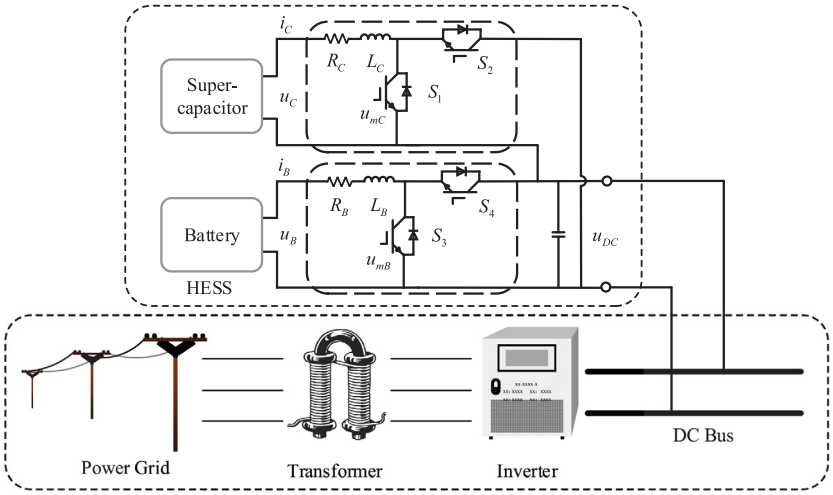


**Fig. 2.** The basic structure of HESS.

Take the super-capacitor as an example, the main control loop and the nonlinear average value model are shown in Fig. 3 where $P_C^*$ is the power command of the super-capacitor after power distribution; $P_r$ is the area capacity; $C_C$ is the total capacitance of super-capacitor system and $u_{C0}$ is the initial voltage of super-capacitor system.

### 2.2. Load frequency control system with hybrid energy storage

One of the important technologies that ensure the frequency quality of the system, a LFC system is designed to ensure that the system frequency remains within an allowable range around the nominal. According to Jaleeli et al. (1992), each area in power grid is composed of AGC system, governor, turbine and rotating mass, and their respective transfer function models are shown in Fig. 4. The HESS system is introduced on the traditional LFC system model established in Jaleeli et al. (1992). The HESS system absorbs or emits power according to the frequency and power deviation of the original LFC system in order to participate in the grid frequency modulation. Therefore, the modified model of the control area $i$ of the load frequency control system including a hybrid energy storage in the multi-area power system is shown in Fig. 4.

The relevant variables and their actual physical meanings are as follows. $\Delta f_i$, $\Delta P_{mi}$, $\Delta P_{gi}$, $\Delta P_{ci}$, and $\Delta P_{tie,i}$ are frequency deviation, generator output power increment, governor valve position increment, unit power command increment, and tie line exchange power deviation, respectively; $T_{gi}$, $T_{ti}$ and $T_{ij}$ are the governor time constant, turbine time constant, and the synchronization coefficient of the tie-line power between different areas, respectively; $H_i$, $D_i$, $R_i$, $\beta_i$ and $K_i$ are the unit inertia, unit damping coefficient, speed control gain, frequency deviation setting and AGC internal PI adjustment control coefficient, respectively.

The following mathematical model is established for the LFC system with HESS:

$$\begin{cases} \dot{x}_i(t) = A_{ii}x_i(t) + B_iu_i(t) + \sum_{j\neq i}^{N} A_{ij}x_j(t) + B_i\Delta P_{di}(t) \\ y_i(t) = C_ix_i(t) \end{cases} \tag{5}$$

where $x_i(t) \triangleq \begin{bmatrix} \Delta f_i & \Delta P_{mi} & \Delta P_{gi} & \Delta P_{ci} & \Delta P_{tie,i} \end{bmatrix}^T$, $C_i \triangleq \begin{bmatrix} 1 & 0 & 0 & 0 & \beta_i \end{bmatrix}$

$$A_{ii} \triangleq \begin{bmatrix} -\frac{D_i}{H_i} & \frac{1}{H_i} & 0 & 0 & -\frac{1}{H_i} \\ 0 & -\frac{1}{T_{ti}} & \frac{1}{T_{ti}} & 0 & 0 \\ -\frac{1}{R_iT_{gi}} & 0 & -\frac{1}{T_{gi}} & \frac{1}{T_{gi}} & 0 \\ -K_i\beta_i & 0 & 0 & 0 & -K_i \\ \sum_{j\neq i}^{N} 2\pi T_{ij} & 0 & 0 & 0 & 0 \end{bmatrix},$$

$$A_{ij} \triangleq \begin{bmatrix} 0 & 0 & 0 & 0 & 0 \\ 0 & 0 & 0 & 0 & 0 \\ 0 & 0 & 0 & 0 & 0 \\ 0 & 0 & 0 & 0 & 0 \\ -2\pi T_{ij} & 0 & 0 & 0 & 0 \end{bmatrix}, B_i \triangleq \begin{bmatrix} -\frac{1}{H_i} \\ 0 \\ 0 \\ 0 \\ 0 \end{bmatrix}.$$

Moreover, $x_i(t)$ is the system state; $u_i(t)$ is the system input from HESS; $y_i(t) \triangleq ACE_i$. $ACE_i$ is the area control error representing the degree of mismatch between electricity power generation and consumption, which is defined as $ACE_i \triangleq \Delta f_i + \beta_i\Delta P_{tie,i}$.

The system (5) can be redefined by considering system parameters uncertainties as follows.

$$\begin{aligned} \dot{x}_i(t) =& (A_{ii} + \Delta A_{ii})x_i(t) + (B_i + \Delta B_i)u_i(t) \\ &+ \sum_{j\neq i}^{N} (A_{ij} + \Delta A_{ij})x_j(t) + (F_i + \Delta F_i)\Delta P_{di}(t) \end{aligned} \tag{6}$$

where $\Delta A_{ii}$, $\Delta B_i$, $\Delta A_{ij}$ and $\Delta F_i$ are the uncertainties of system parameters.

Using $g_i(t)$ as the aggregated uncertainties

$$g_i(t) = \Delta A_{ii}x_i(t) + \Delta B_iu_i(t) + \sum_{j\neq i}^{N} \Delta A_{ij}x_j(t) + (F_i + \Delta F_i)\Delta P_{di}(t)$$

Then, the system model in (5) becomes

$$\begin{cases} \dot{x}_i(t) = A_{ii}x_i(t) + B_iu_i(t) + \sum_{j\neq i}^{N} A_{ij}x_j(t) + g_i(t) \\ y_i(t) = C_ix_i(t) \end{cases} \tag{7}$$

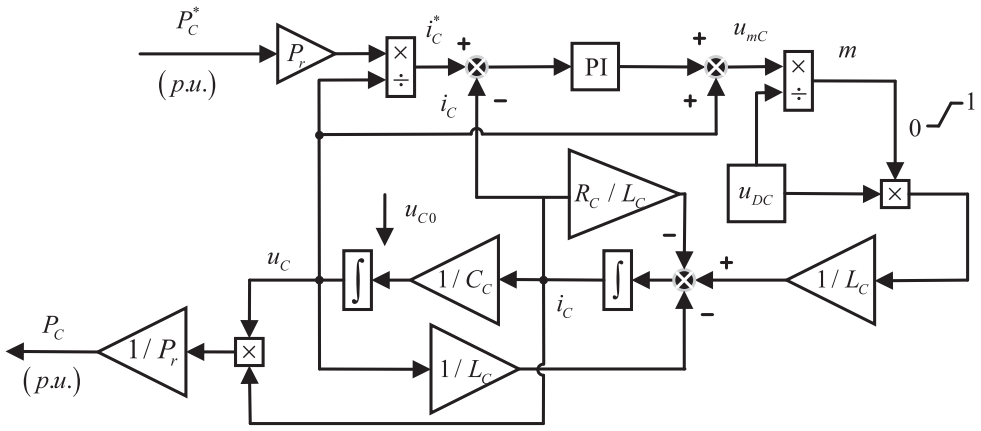


**Fig. 3.** Model of the super-capacitor and its primary control loop.

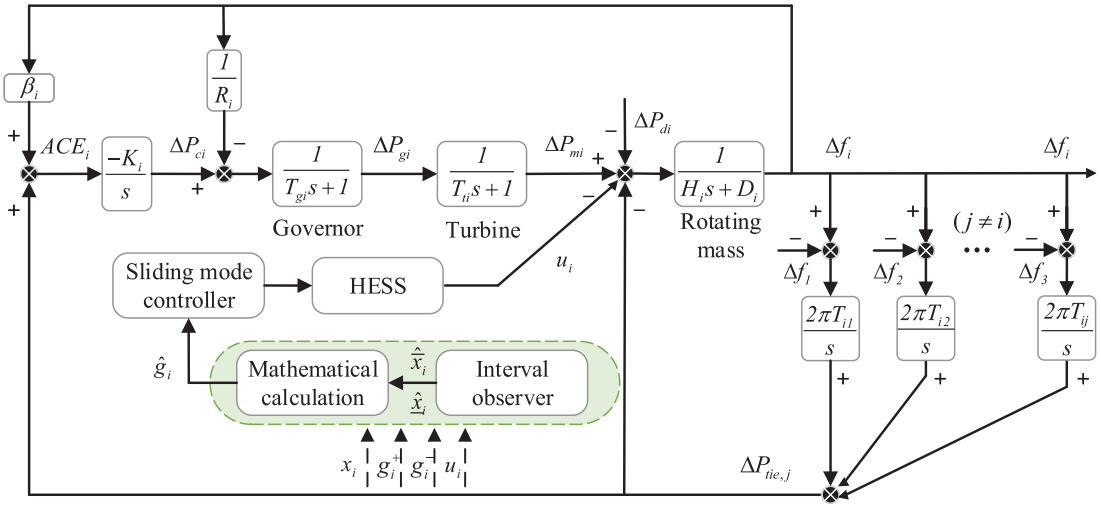


**Fig. 4.** Control model of the $i$th area.

**Definition 1** (*Li et al., 2019*). The Metzler matrix is defined as square matrix whose non-diagonal components are non-negative. The Hurwitz matrix is defined as a square matrix with all eigenvalues having strictly negative real parts.

**Lemma 1** (*Efimov et al., 2013*). *The system* $\dot{x}(t) = Ax(t) + \omega(t)$ *with Metzler matrix A, has* $x(t) \geq 0$ *for all* $t > 0$ *in the condition of* $x(0) > 0, \omega(t) > 0$.

**Assumption 1.** All the information of system state can be measured.

**Assumption 2.** There exists $g_i^+ > 0$ and $g_i^- < 0$ such that $g_i^- \leq g_i(t) \leq g_i^+$.

## 3. Interval disturbance reconstruction based sliding mode control strategy

In this section, by designing an interval observer, online estimation of the upper and lower boundary values of the interconnected power system state is used to reconstruct the uncertainty term $g_i(t)$ of the system. Combined with the reconstruction value of the uncertainty term $g_i(t)$, a sliding mode load frequency controller based on disturbance reconstruction is then designed to ensure that the power system frequency can meet good transient and steady-state performance under load changes and uncertain parameters.

### 3.1. Design of interval observer

Interval observer usually consists of two subsystems, and estimates interval boundary values of the real state by assuming the maximum and minimum bounds of the unknown input in the system.

According to the system (7), an interval observer of the following form is designed:

$$\begin{cases} \dot{\hat{\overline{x}}}_i(t) = A_{ii}x_i(t) + B_iu_i(t) + \sum_{j\neq i}^{N} A_{ij}x_j(t) + g_i^+ \\ \qquad -g_i^- + L_i(x_i(t) - C_i\hat{\overline{x}}_i(t)) \\ \dot{\hat{\underline{x}}}_i(t) = A_{ii}x_i(t) + B_iu_i(t) + \sum_{j\neq i}^{N} A_{ij}x_j(t) + g_i^- \\ \qquad -g_i^+ + L_i(x_i(t) - C_i\hat{\underline{x}}_i(t)) \end{cases} \tag{8}$$

where $\hat{\overline{x}}_i(t)$ and $\hat{\underline{x}}_i(t)$ are the states of interval observer. $L_i$ is the interval observer gain coefficient that needs to be set in advance.

**Theorem 1.** *In the case of satisfying Assumption 1, if the interval observer hold the following initial conditions:*

$$\hat{\underline{x}}_i(0) \leq x_i(0) \leq \hat{\overline{x}}_i(0) \tag{9}$$

*then (8) can get the information about the interval bounds of the system state with* $-L_i$ *set to be a Metzler and Hurwitz matrix.*

**Proof of Theorem 1.** Define interval observer estimation errors of the system state $x_i(t)$ as

$$e_{1i}(t) = \hat{\bar{x}}_i(t) - x_i(t)$$
$$e_{1i}(t) = x_i(t) - \hat{\underline{x}}_i(t)$$

Combining Eqs. (7) and (8), the following error dynamic systems can be obtained:

$$\begin{aligned} \dot{e}_{1i}(t) &= g_i^+ - g_i^- - g_i(t) - L_i e_{1i}(t) \\ \dot{e}_{2i}(t) &= -g_i^- + g_i^+ + g_i(t) - L_i e_{2i}(t) \end{aligned} \tag{10}$$

According to Assumption 1, we can get the following conclusions:

$$g_i^+ - g_i^- - g_i(t) \geq 0$$
$$-g_i^- + g_i^+ + g_i(t) \geq 0$$

Combining with Lemma 1, as long as $-L_i$ chosen as a Metzler and Hurwitz matrix, we can get that for $t > 0$, there always have $\hat{\underline{x}}_i(t) \leq x_i(t) \leq \hat{\bar{x}}_i(t)$, therefore, (8) is an interval observer of the system (7). Where $-L_i$ chosen as a Hurwitz matrix ensures the stability of the error dynamic systems. □

### 3.2. Interval observer based disturbance reconstruction

According to Theorem 1, when the condition is met, for all $t > 0$, it always has $\hat{\underline{x}}_i(t) \leq x_i(t) \leq \hat{\bar{x}}_i(t)$, so the system state $x_i(t)$ and its upper and lower boundary estimations satisfy the following relationship

$$x_i(t) = \Phi_i(t)\hat{\bar{x}}_i(t) + (I - \Phi_i(t))\hat{\underline{x}}_i(t) \tag{11}$$

where $\Phi_i(t) = diag\{a_1(t), a_2(t), \ldots, a_n(t)\}$ and $0 \leq a_i(t) \leq 1, i = 1, 2, \ldots, n$.

Therefore, the interval observer obtained by Theorem 1 can be used to reconstruct the system uncertain term $g_i(t)$.

**Theorem 2.** *For the model of LFC system with HESS (7), according to the interval observer designed by Theorem 1, the system uncertain term $g_i(t)$ can be reconstructed by the following algebraic calculation,*

$$\hat{g}_i(t) = M_1\hat{\bar{x}}_i(t) - M_1\hat{\underline{x}}_i(t) + M_2(g_i^+ - g_i^-) \tag{12}$$

*where $M_1$ and $M_2$ are respectively defined as:*

$$M_1 = \Phi_i(t)N_1 + (I - \Phi_i(t))N_2 + \dot{\Phi}_i(t) - A_{ii}\Phi_i(t)$$
$$M_2 = 2\Phi_i(t) - I$$

*moreover,*

$$N_1 = A_{ii}\Phi_i(t) + L_i\Phi_i(t) - L_i$$
$$N_2 = A_{ii}\Phi_i(t) + L_i\Phi_i(t)$$

**Proof of Theorem 2.** According to (8) and formula (11), we can get:

$$\begin{aligned} \dot{\hat{\bar{x}}}_i(t) =& N_1\hat{\bar{x}}_i(t) + (A_{ii} - N_1)\hat{\underline{x}}_i(t) + B_i u_i(t) + g_i^+ - g_i^- + \\ & \sum_{j\neq i}^{N} A_{ij}(\Phi_j(t)\hat{\bar{x}}_j(t) + (I - \Phi_j(t))\hat{\underline{x}}_j(t)) \\ \dot{\hat{\underline{x}}}_i(t) =& N_2\hat{\bar{x}}_i(t) + (A_{ii} - N_2)\hat{\underline{x}}_i(t) + B_i u_i(t) + g_i^- - g_i^+ + \\ & \sum_{j\neq i}^{N} A_{ij}(\Phi_j(t)\hat{\bar{x}}_j(t) + (I - \Phi_j(t))\hat{\underline{x}}_j(t)) \end{aligned} \tag{13}$$

According to the (11), the first derivative of $x_i(t)$ is

$$\begin{aligned} \dot{x}_i(t) =& (\Phi_i(t)N_1 + (I - \Phi_i(t))N_2 + \dot{\Phi}_i(t))\hat{\bar{x}}_i(t) + B_i u_i(t) \\ & + (A_{ii} - \Phi_i(t)N_1 - (I - \Phi_i(t))N_2 - \dot{\Phi}_i(t))\hat{\underline{x}}_i(t) \\ & + \sum_{j\neq i}^{N} A_{ij}(\Phi_j(t)\hat{\bar{x}}_j(t) + (I - \Phi_j(t))\hat{\underline{x}}_i(t)) \\ & + (2\Phi_i(t) - I)(g_i^+ - g_i^-) \end{aligned} \tag{14}$$

After comparing the system dynamic equation (7) with (14), we can get the expression of the uncertain term:

$$\begin{aligned} g_i(t) =& (\Phi_i(t)N_1 + (I - \Phi_i(t))N_2 + \dot{\Phi}_i(t) - A_{ii}\Phi_i(t))(\hat{\bar{x}}_i(t) - \hat{\underline{x}}_i(t)) \\ & + (2\Phi_i(t) - I)(g_i^+ - g_i^-) \end{aligned} \tag{15}$$

By defining

$$M_1 = \Phi_i(t)N_1 + (I - \Phi_i(t))N_2 + \dot{\Phi}_i(t) - A_{ii}\Phi_i(t)$$
$$M_2 = 2\Phi_i(t) - I$$

we can get

$$g_i(t) = M_1\hat{\bar{x}}_i(t) - M_1\hat{\underline{x}}_i(t) + M_2(d_i^+ - d_i^-)$$

Obviously, in order to calculate the uncertain term $g_i(t)$, it is a inevitable prerequisite to get the value of $\Phi_i(t)$ and $\dot{\Phi}_i(t)$, we can calculate $\Phi_i(t)$ by the following equivalent conversion formula (16)

$$\begin{aligned} x_i(t) =& \begin{bmatrix} \hat{\bar{x}}_{i1} & & & \\ & \hat{\bar{x}}_{i2} & & \\ & & \ddots & \\ & & & \hat{\bar{x}}_{in} \end{bmatrix} \begin{bmatrix} a_1(t) \\ a_2(t) \\ \vdots \\ a_n(t) \end{bmatrix} \\ & + \begin{bmatrix} \hat{\underline{x}}_{i1} & & & \\ & \hat{\underline{x}}_{i2} & & \\ & & \ddots & \\ & & & \hat{\underline{x}}_{in} \end{bmatrix} \begin{bmatrix} 1 - a_1(t) \\ 1 - a_2(t) \\ \vdots \\ 1 - a_n(t) \end{bmatrix} \end{aligned} \tag{16}$$

Define

$$Q_1(t) = diag\left\{ \begin{array}{cccc} \hat{\bar{x}}_{i1} & \hat{\bar{x}}_{i2} & \cdots & \hat{\bar{x}}_{in} \end{array} \right\}$$
$$Q_2(t) = diag\left\{ \begin{array}{cccc} \hat{\underline{x}}_{i1} & \hat{\underline{x}}_{i2} & \cdots & \hat{\underline{x}}_{in} \end{array} \right\}$$
$$a_v(t) = \left[ \begin{array}{cccc} a_1(t) & a_2(t) & \cdots & a_n(t) \end{array} \right]^T$$

then we can get

$$(Q_1(t) - Q_2(t))a_v(t) = x_i(t) - \hat{\underline{x}}_i(t) \tag{17}$$

$$a_v(t) = (Q_1(t) - Q_2(t))^{-1}(x_i(t) - \hat{\underline{x}}_i(t)) \tag{18}$$

Because of $\Phi_i(t) = diag\{ \begin{array}{cccc} a_1(t) & a_2(t) & \cdots & a_n(t) \end{array} \}$, $\Phi_i(t)$ and $\dot{\Phi}_i(t)$ can be calculated. So it proves that the system uncertain term $g_i(t)$ can be reconstructed online by (12). □

### 3.3. Design of sliding mode load frequency controller

In order to maintain the active power balance of the power grid when the system parameters are uncertain and load disturbances occur, a sliding mode load frequency controller based on interval disturbance reconstruction has been designed in this section.

Consider the following form of sliding surface,

$$s_i(t) = C_i x_i(t) \tag{19}$$

It is further obtained that,

$$\dot{s}_i(t) = C_i\dot{x}_i(t) = C_i(A_{ii}x_i(t) + B_iu_i(t) + \sum_{j\neq i}^{N} A_{ij}x_j(t) + g_i(t)) \tag{20}$$

Selecting the sliding mode reaching law as follows

$$\dot{s}_i(t) = -\varepsilon_i sgn(s_i(t)) \tag{21}$$

The interval disturbance reconstruction based sliding mode controller is designed as

$$u_i(t) = -(C_iB_i)^{-1}\left[C_i\hat{g}_i(t) + C_iA_{ii}x_i(t) + C_i\sum_{j\neq i}^{N} A_{ij}x_j(t) + \varepsilon_i sign(s_i(t))\right] \tag{22}$$

define $\tilde{g}_i(t) = g_i(t) - \hat{g}_i(t)$, design $\left|C_i\tilde{g}_i(t)\right| \leq \varepsilon_i$

Design the Lyapunov function as

$$V_i(t) \triangleq \frac{1}{2}s_i^2(t) \tag{23}$$

It is further obtained that,

$$\begin{aligned}
\dot{V}_i(t) =& s_i(t)\dot{s}_i(t) = s_i(t)\left[C_i(A_{ii}x_i(t) + B_iu_i(t) + \sum_{j\neq i}^{N} A_{ij}x_j(t) + g_i(t))\right] \\
=& s_i(t)\left[C_iA_{ii}x_i(t) - (C_i\hat{g}_i(t) + C_iA_{ii}x_i(t) + C_i\sum_{j\neq i}^{N} A_{ij}x_j(t) + \varepsilon_i sign(s_i(t))) + C_i\sum_{j\neq i}^{N} A_{ij}x_j(t) + C_ig_i(t)\right] \\
=& s_i(t)\left[C_i(g_i(t) - \hat{g}_i(t)) - \varepsilon_i sign(s_i(t))\right] \\
=& s_i(t)C_i\tilde{g}_i(t) - \varepsilon_i\left|s_i(t)\right| \\
\leq& \left|C_i\tilde{g}_i(t)\right|\left|s_i(t)\right| - \varepsilon_i\left|s_i(t)\right| \\
\leq& 0
\end{aligned}$$

Consider the Lyapunov function as $V_i(t) = \frac{1}{2}s_i^2(t)$, then $\dot{V}_i(t) = s_i(t)\dot{s}_i(t) \leq 0$. When $\dot{V}_i(t) \equiv 0$, $s_i(t) \equiv 0$. According to the principle of LaSalle invariance, the system tends to be stable.

## 4. Simulation results

In order to further study the effectiveness of the interval disturbance reconstruction sliding mode control strategy with hybrid energy storage proposed in this paper, the following simulation experiments are used. A three-area power grid including a HESS model is built as a fifth-order linear system with uncertainties in the MATLAB/Simulink platform. The simulation experiment is analyzed, and the simulation time is 100 s. Table 1 shows the established system parameters (Su et al., 2018).

Taking area 1 as an example, the parameters and initial values in the design interval observer and controller are shown in Table 2. This paper takes 10 MW as the benchmark value, assuming that the initial state of the system is working in a balance between power generation and power consumption.

Different load disturbances are added in each control area. We can get the simulation results from Figs. 5–7(a). To illustrate the influence of the disturbance bound on the interval estimation and disturbance reconstruction performance, another set of disturbance bound $g_i^+ = [0.02; 0.02; 0.02; 0.02; 0.02]$, $g_i^- = -g_i^+$ is used for comparison experiment. Fig. 5 shows the interval estimations of the system frequency deviation and the tie line power deviation from interval observers. The interval observer can effectively track the boundaries of system state, and the size of the interval is related to $g_i^+$ and $g_i^-$. When the value of $g_i^+$ is 0.02, the interval estimate is bounded by the green lines while the results for $g_i^+ = 0.01$ is bounded by blue lines. It can be found from Fig. 5 that the larger the value of the disturbance bound is, the larger the size of the interval will appear.

Fig. 6(a) shows the reconstruction of external load disturbances in different control areas, which shows that the reconstructed disturbances accurately and quickly track the external load disturbances. In addition, under different disturbance bounds, the disturbance reconstruction results are similar. This shows that different disturbance bounds will lead to the same disturbance reconstruction results, which facilitates the choice of parameters.

The real-time disturbance reconstruction value obtained through interval disturbance reconstruction is used to design the sliding mode controller proposed in this paper. In order to deeper study the effectiveness of the designed sliding mode control method with HESS, the following three simulation cases were performed. Case 1: HESS participates in load frequency control with the control strategy proposed in this paper. Case 2: HESS does not participate in load frequency control. Case 3: HESS participates in load frequency control with PI controller.

The comparison between the simulation results of the three control strategies are shown in Figs. 6(b)–7(a). Fig. 6(b) shows the frequency response in each grid under the different control strategies, while Fig. 7(a) shows the power deviation on the tie line in each area under the different control strategies. It can be found from the comparison experiments that under the influence of the same load disturbances, the traditional load frequency controller cannot quickly respond to the change of the load disturbances when the HESS does not participate in the frequency modulation. The resulting frequency deviations and tie line power deviations are large, and it is difficult to ensure the stable operation of the system. However, when HESS participates in frequency modulation, because the control strategy proposed in this paper can effectively reconstruct load disturbances in real time, it responds to load changes effectively and quickly, and maintains the system frequency deviation within a small range. Its control effect is better than PI controller.

In order to further demonstrate the control performance of the proposed control strategy, the disturbance observer-based sliding mode control methods in Wang et al. (2018), Mi et al. (2016), Yang et al. (2019) are applied to the multi-area interconnected power system at the same time, and the comparison results are shown in Figs. 7(b)–8(b).

In Fig. 7(b), the reconstruction values of the disturbance from disturbance observer method and the proposed disturbance reconstruction method were compared. It can be obtained that the proposed method has a slight overshoot, but it can quickly track the actual disturbances. However, although the disturbance observer method shows no overshoot, it has a longer response time, which indicates the disturbance observer-based method in Wang et al. (2018), Mi et al. (2016), Yang et al. (2019) requires more time to stabilize the tracking error.

The comparison results between proposed control method and the sliding mode control based on disturbance observer method and PI method are shown in Fig. 8. Fig. 8(a) shows the frequency

**Table 1**
System parameters.

| Area i | $D_i$ (p.u./Hz) | $H_i$ (p.u s) | $T_{ti}$ (s) | $T_{gi}$ (s) | $R_i$ (Hz/p.u.) | $K_i$ | $\beta_i$ (Hz/p.u.) |
|---|---|---|---|---|---|---|---|
| 1 | 0.025 | 0.3708 | 0.19 | 0.05 | 2.15 | 0.6 | 0.49 |
| 2 | 0.025 | 0.2708 | 0.23 | 0.05 | 2.45 | 0.6 | 0.43 |
| 3 | 0.025 | 0.2708 | 0.23 | 0.05 | 2.45 | 0.6 | 0.43 |
| $T_{12} = 0.13$, $T_{13} = 0.12$, $T_{23} = 0.10$ (p.u./Hz) | | | | | | | |

**Table 2**
The parameters and initial values of interval observer and controller in area 1.

| Module | Parameters |
|---|---|
| Controller | $\varepsilon_1 = 0.01$ |
| Interval observer | $L_1 = \begin{bmatrix} 5 & -1 & -1 & -1 & -1 \\ -1 & 5 & -1 & -1 & -1 \\ -1 & -1 & 5 & -1 & -1 \\ -1 & -1 & -1 & 5 & -1 \\ -1 & -1 & -1 & -1 & 5 \end{bmatrix}$<br>$g_1^+ = [0.01; 0.01; 0.01; 0.01; 0.01]$, $g_1^- = -g_1^+$<br>$\hat{\bar{x}}_1(0) = [0.005; 0.005; 0.005; 0.005; 0.005]$, $\hat{\underline{x}}_1(0) = -\hat{\bar{x}}_1(0)$ |

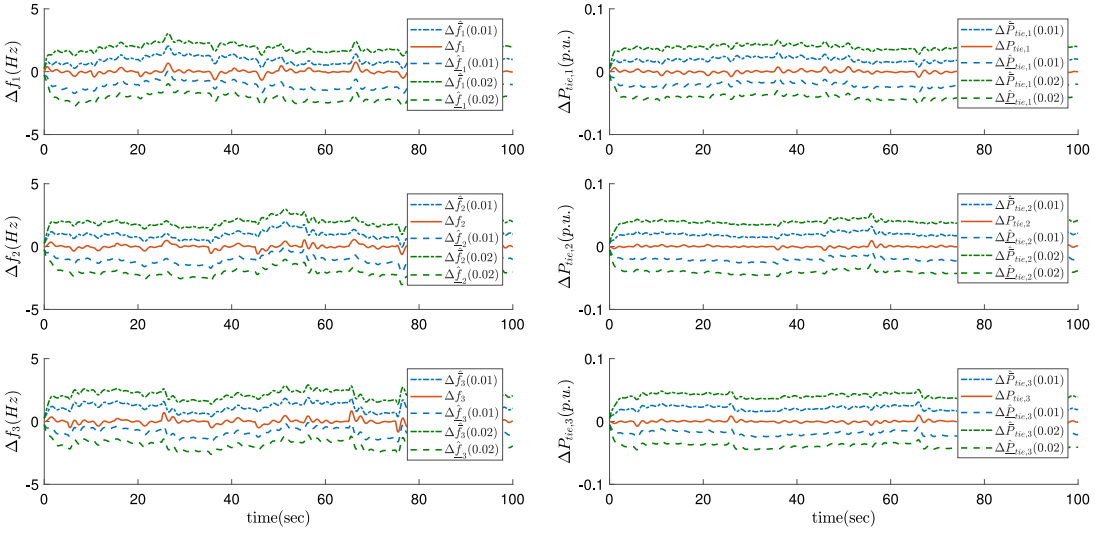


(a) (b)

**Fig. 5.** Simulation results. (a) The interval estimation for $\Delta f_i(t)$ in each power grid. (b) The interval estimation for $\Delta P_{tie,i}(t)$ in each power grid.

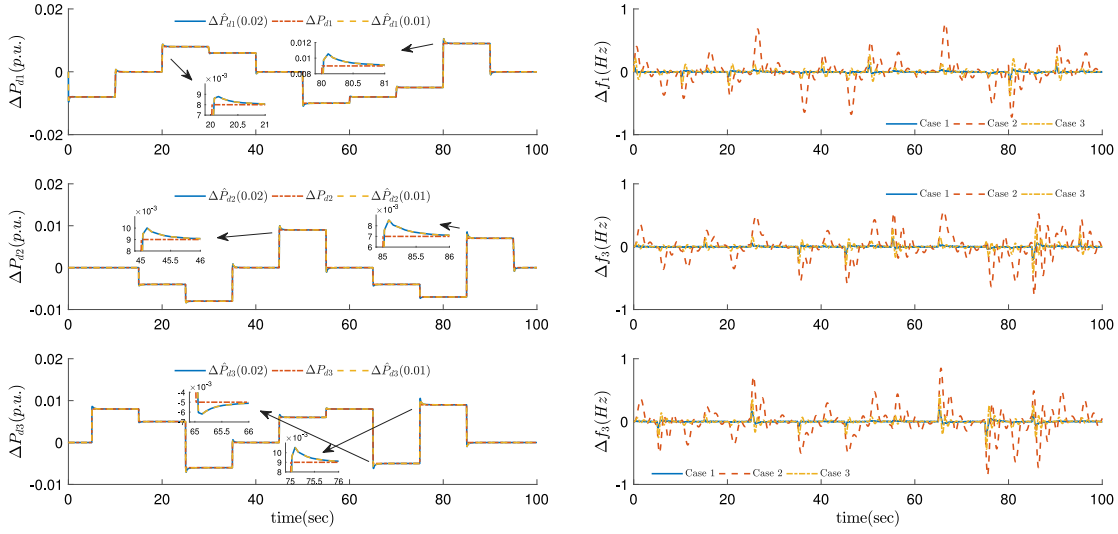


(a) (b)

**Fig. 6.** Simulation results. (a) The reconstruction values of $\Delta P_{di}(t)$ in each area. (b) $\Delta f_i(t)$ in each power grid under load disturbances.

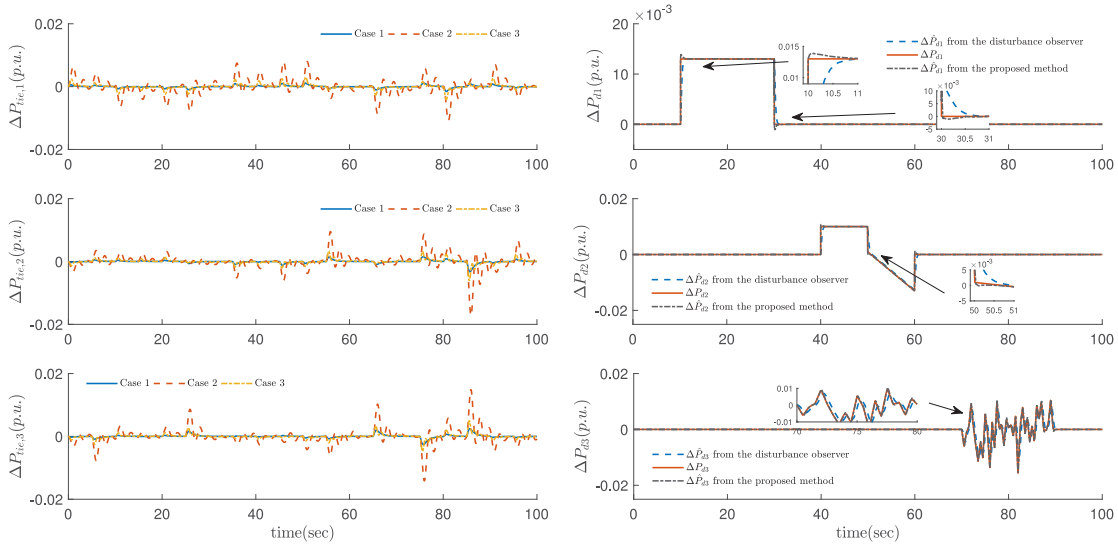


**Fig. 7.** Simulation results. (a) $\Delta P_{tie,i}(t)$ in each power grid under load disturbances. (b) The estimation values of $\Delta P_{di}(t)$ in each area.

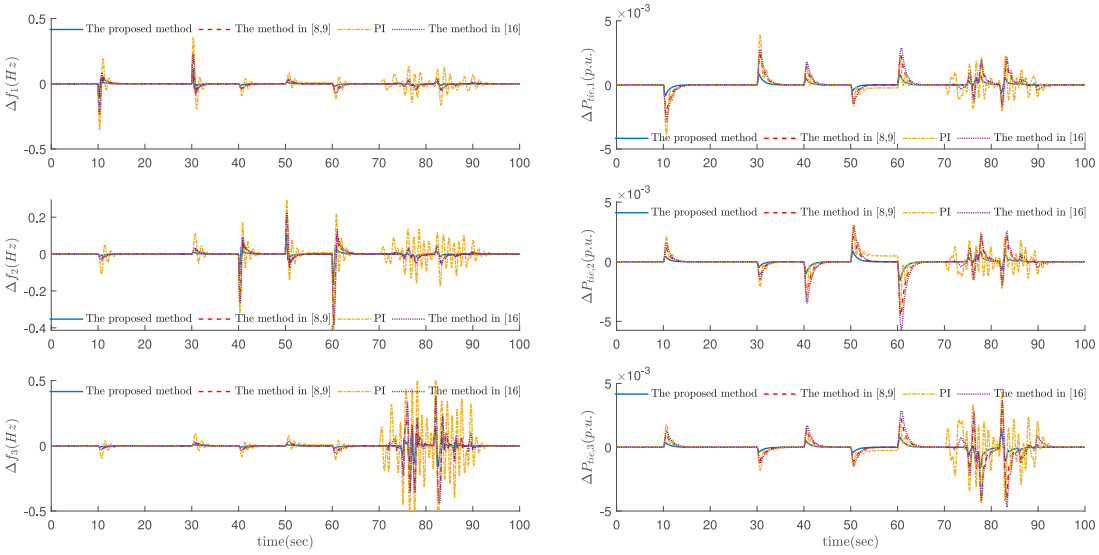


**Fig. 8.** Simulation results. (a) $\Delta f_i(t)$ in each power grid under load disturbances. (b) $\Delta P_{tie,i}(t)$ in each power grid under load disturbances.

response in each grid under the different control strategies, while Fig. 8(b) shows the power deviation on the tie line in each area under the different control strategies. Through comparative experiments, it can be found that the PI controller cannot quickly respond to the change in load disturbances. The resulting frequency deviations and tie line power deviations are large, and it is difficult to ensure the stable operation of the system. Compared with the methods in Wang et al. (2018), Mi et al. (2016), Yang et al. (2019), the control strategy proposed in this paper has better dynamic performance with quicker convergence rate and better anti-disturbance performance owing to the high estimation precision of interval observer which exhibits input decoupled characteristic. Besides, the parameter adjustment of the proposed control strategy is easier to implement by ensuring the initial state in the prescribed interval boundary. The simulation results in Fig. 8 show that it can quickly suppress frequency fluctuation and better improve the system performance.

## 5. Conclusion

A sliding mode control strategy based on interval observer has been designed for LFC issue of the multi-area interconnected power system with HESS in this paper. Compared with some disturbance observer-based methods, the proposed control strategy can stabilize the frequency fluctuation more quickly and effectively due to the interval observer-based disturbance reconstruction approach. First, the system state is accurately estimated via the designed interval observer. Based on the estimation information, the disturbance of each area is estimated with high precision by the proposed input decoupled reconstruction method. Moreover, the sliding mode controller, which takes the load disturbances into account, supplies the desired and appropriate power flow reference for HESS, and the HESS effectively participates in frequency modulation under the proposed control strategy so that the stability of the power grids is ensured and the

system frequency and tie-line power fluctuations are maintained within a small range.

In the future research work, we will carry out in-depth research on improving technical route of control strategy against some important nonlinearities such as generation rate constraint, governor deadband, and time delay in the communication channel in LFC system.

## Declaration of competing interest

The authors declare that they have no known competing financial interests or personal relationships that could have appeared to influence the work reported in this paper.

## Acknowledgments

The authors are very grateful to the anonymous reviewers and the editor for their constructive suggestions. This work was partially supported by the National Natural Science Foundation of China (61973140), Beijing Natural Science Foundation (21JC0026) and State Grid Integrated Energy Service Group Science and Technology Project (Research on Key Technologies of system integration of large capacity energy storage power station).

## References

Alhelou, H.H., Golshan, M.E.H., 2018. Challenges and opportunities of load frequency control in conventional, modern and future smart power systems: A comprehensive review. Energies 11 (10), 1–35.

Alhelou, H.H., Golshan, M.E.H., 2019. A decentralized functional observer based optimal LFC considering unknown inputs, uncertainties, and cyber-attacks. IEEE Trans. Power Syst. 34 (6), 4408–4417.

Alhelou, H.H., Golshan, M.E.H., 2020. Deterministic dynamic state estimation-based optimal LFC for interconnected power systems using unknown input observer. IEEE Trans. Smart Grid 11 (2), 1582–1592.

Ameli, A., Hooshyar, A., 2018. Attack detection and identification for automatic generation control systems. IEEE Trans. Power Syst. 33 (5), 4760–4774.

Efimov, D., Perruquetti, W., Raïssi, T., Zolghadri, A., 2013. Interval observers for time-varying discrete-time systems. IEEE Trans. Automat. Control 58 (12), 3218–3224.

Gholami, K., Parvaneh, M.H., 2019. A mutated salp swarm algorithm for optimum allocation of active and reactive power sources in radial distribution systems. Appl. Soft Comput. 85, 105833.

Jaleeli, N., VanSlyck, L.S., Ewart, D.N., Fink, L.H., Hoffmann, A.G., 1992. Understanding automatic generation control. IEEE Trans. Power Syst. 7 (3), 1106–1122.

Li, J., Wang, Z., Raïssi, T., Shen, Y., 2019. Interval observer design for continuous-time linear parameter-varying systems. Systems Control Lett. 134, 104541.

Mi, Y., Fu, Y., Li, D., Wang, C., Loh, P.C., Wang, P., 2016. The sliding mode load frequency control for hybrid power system based on disturbance observer. Int. J. Electr. Power Energy Syst. 74, 446–452.

Onyeka, A.E., Yan, X.G., Mao, Z., Jiang, B., 2020. Robust decentralised load frequency control for interconnected time delay power systems using sliding mode techniques. IET Control Theory Appl. 14 (3), 470–480.

Parvaneh, M.H., Khorasani, P.G., 2020. A new hybrid method based on fuzzy logic for maximum power point tracking of photovoltaic systems. Energy Rep. 6, 1619–1632.

Rahmani, M., Sadati, N., 2013. Hierarchical optimal robust load-frequency control for power systems. IET Gener. Transm. Distrib. 6 (4), 303–312.

Rerkpreedapong, D., Hasanovic, A., Feliachi, A., 2003. Robust load frequency control using genetic algorithms and linear matrix inequalities. IEEE Trans. Power Syst. 18 (2), 855–861.

Rubaai, A., Udo, V., 1992. An adaptive control scheme for load-frequency control of multiarea power systems Part I. Identification and functional design. Electr. Power Syst. Res. 24 (3), 183–188.

Saikia, L., Nanda, J., Mishra, S., 2011. Performance comparison of several classical controllers in AGC for multi-area interconnected thermal system. Int. J. Electr. Power Energy Syst. 33 (3), 394–401.

Su, Q., Fan, Z., Lu, T., Long, Y., Li, J., 2020. Fault detection for switched systems with all modes unstable based on interval observer. Inform. Sci. 517, 167–182.

Su, X., Liu, X., Song, Y., 2018. Fault-tolerant control of multiarea power systems via a sliding-mode observer technique. IEEE/ASME Trans. Mechatronics 23 (1), 38–47.

Tian, Y., Zhang, K., Jiang, B., Yan, X., 2020. Interval observer and unknown input observer-based sensor fault estimation for high-speed railway traction motor. J. Franklin Inst. B 357 (2), 1137–1154.

Tungadio, D.H., Sun, Y., 2019. Load frequency controllers considering renewable energy integration in power system. Energy Rep. 5, 436–453.

Wang, C., Mi, Y., Fu, Y., Wang, P., 2018. Frequency control of an isolated microgrid using double sliding mode controllers and disturbance observer. IEEE Trans. Smart Grid 9 (2), 923–930.

Wood, A.J., Wollenberg, B.F., 2012. Power Generation, Operation, and Control. Wiley, New York, NY, USA.

Xu, D., Liu, J., Yan, X., Yan, W., 2018. A novel adaptive neural network constrained control for a multi-area interconnected power system with hybrid energy storage. IEEE Trans. Ind. Electron. 65 (8), 6625–6634.

Yan, W., Sheng, L., Xu, D., Yang, W., 2018. $H_\infty$ Robust load frequency control for multi-area interconnected power system with hybrid energy storage system. Appl. Sci. 8 (10), 1748.

Yang, W., Yu, D., Xu, D., Zhang, Y., 2019. Observer-based sliding mode FTC for multi-area interconnected power systems against hybrid energy storage faults. Energies 12 (14), 2819.

Zammali, C., Gorp, J.V., Wang, Z., Raissi, T., 2020. Sensor fault detection for switched systems using interval observer with $L_\infty$ performance. Eur. J. Control 57, 147–156.

Zhang, Z., Yang, G., 2017. Fault detection for discrete-time LPV systems using interval observers. Internat. J. Systems Sci. 48 (14), 2921–2935.

Zhou, X., Wang, Y., Zhang, W., Yang, W., Zhang, Y., Xu, D., 2020. Actuator fault-tolerant load frequency control for interconnected power systems with hybrid energy storage system. Energy Rep. 6 (9), 1312–1317.